The Astrophysical Journal Letters, 918:L13 (6pp), 2021 September 1 https://doi.org/10.3847/2041-8213/ac1e9a

Measurements of the Magnetic Field Strengths at the Bases of Stellar Coronae Using the Magnetic-field-induced Transition Theory

Yajie Chen[1], Xianyu Liu[1], Hui Tian[1,2], Xianyong Bai[2,3], Meng Jin[4], Wenxian Li[2], Yang Yang[5,6], Zihao Yang[1], and Yuanyong Deng[2,3]

[1] School of Earth and Space Sciences, Peking University, 100871 Beijing, People's Republic of China; huitian@pku.edu.cn
[2] Key Laboratory of Solar Activity, National Astronomical Observatories, Chinese Academy of Sciences, Beijing 100012, People's Republic of China; xybai@bao.ac.cn
[3] School of Astronomy and Space Science, University of Chinese Academy of Sciences, Beijing 100049, People's Republic of China
[4] SETI Institute, 189 N Bernardo Avenue, Suite 200, Mountain View, CA 94043, USA
[5] Shanghai EBIT laboratory, Institute of Modern Physics, Fudan University, Shanghai, People's Republic of China
[6] Key Laboratory of Nuclear Physics and Ion-beam Application (MOE), Fudan University, Shanghai 200433, People's Republic of China
Received 2021 July 7; revised 2021 August 11; accepted 2021 August 18; published 2021 August 27

Abstract

Measurements of the magnetic field in the stellar coronae are extremely difficult. Recently, it was proposed that the magnetic-field-induced transition (MIT) of the Fe X 257 Å line can be used to measure the coronal magnetic field of the Sun. We performed forward modeling with a series of global stellar magnetohydrodynamics models to investigate the possibility of extending this method to other late-type stars. We first synthesized the emissions of several Fe X lines for each stellar model, then calculated the magnetic field strengths using the intensity ratios of Fe X 257 Å to several other Fe X lines based on the MIT theory. Finally, we compared the derived field strengths with those in the models, and concluded that this method can be used to measure at least the magnetic field strengths at the coronal bases of stars with a mean surface magnetic flux density about one order of magnitude higher than that of the Sun. Our investigation suggests the need for an extreme ultraviolet spectrometer to perform routine measurements of the stellar coronal magnetic field.

Unified Astronomy Thesaurus concepts: Magnetohydrodynamics (1964); Stellar coronae (305); Stellar magnetic fields (1610)

1. Introduction

There is increasing consensus that the magnetic activity of a host star, e.g., strong X-ray and ultraviolet emission, stellar wind, superflares, and coronal mass ejections (e.g., Baranov 1990; Haisch et al. 1991; Maehara et al. 2012; Alvarado-Gómez et al. 2018; Argiroffi et al. 2019; Veronig et al. 2021) could cause atmospheric loss (e.g., Lammer et al. 2003; Dong et al. 2017) and surface sterilization (e.g., Segura et al. 2010; Tabataba-Vakili et al. 2016) of exoplanets, and thus significantly affect the exoplanet habitability (e.g., Linsky 2019). The energy source of these different types of stellar activities lies mainly in the magnetic field (e.g., Yokoyama & Shibata 1998; Pevtsov et al. 2003). So measurements of the stellar magnetic field are important for both the stellar atmospheric characterization and the search for extraterrestrial life.

The Zeeman effect is often used to derive the average magnetic field strengths on stellar surfaces (photospheres) from observations of the integrated spectral line profiles (e.g., Reiners & Basri 2010; Reiners 2012). Furthermore, the Zeeman–Doppler imaging technique has been applied to obtain large-scale magnetic field distributions in the photospheres of some stars (e.g., Semel 1989; Rosén et al. 2015).

Measurements of the magnetic field above the stellar surfaces are very rare. After all, routine magnetic field measurements of the solar corona are still missing (e.g., Lin et al. 2004; Liu & Lin 2008; Chen et al. 2018, 2020; Li et al. 2017; Gary et al. 2018; Zhao et al. 2019, 2021; Yang et al. 2020a, 2020b; Fleishman et al. 2020; Zhu et al. 2021). So far, only a few attempts have been made to obtain information on the stellar coronal magnetic field. One approach is to construct the global magnetic field structures using the technique of magnetic field extrapolation based on the Zeeman–Doppler maps observed in the stellar photospheres (e.g., Jardine et al. 2002; Kochukhov & Piskunov 2002; Donati et al. 2006; Petit et al. 2008; Johnstone et al. 2014). However, the Zeeman–Doppler maps can only reveal large-scale structures, and they are subject to large uncertainties, especially when the stellar spin axes are not perpendicular to the lines of sight (e.g., Lehmann et al. 2019). Moreover, magnetic field extrapolations usually rely on several assumptions, e.g., the magnetic field is potential, which are often not valid in stellar atmospheres (Wiegelmann & Sakurai 2021).

Another approach is to infer the magnetic field strengths of stellar coronae from radio observations (e.g., Gary & Linsky 1981; Mutel et al. 1985; Güdel 2002). These observations often yielded a field strength of several hundred Gauss, which is likely for the core of active regions (ARs) or flare regions on the observed stars. However, the radio emission mechanisms, which are critical for the determination of the field strengths, are not always evident from observations. In addition, quiescent radio emission has not been detected on many late-type stars (White 1996).

Recently, Li et al. (2015, 2016) suggested that the intensity ratios of several Fe X lines can be used to measure the solar coronal magnetic field based on the magnetic-field-induced transition (MIT) theory. The suitability of this method for measurements of the solar coronal magnetic field has been recently demonstrated by Chen et al. (2021) through a forward modeling approach. This technique has also been successfully applied to solar extreme ultraviolet (EUV) spectral observations (e.g., Si et al. 2020; Landi et al. 2020, 2021; Brooks & Yardley 2021). The measured field strengths in solar ARs are

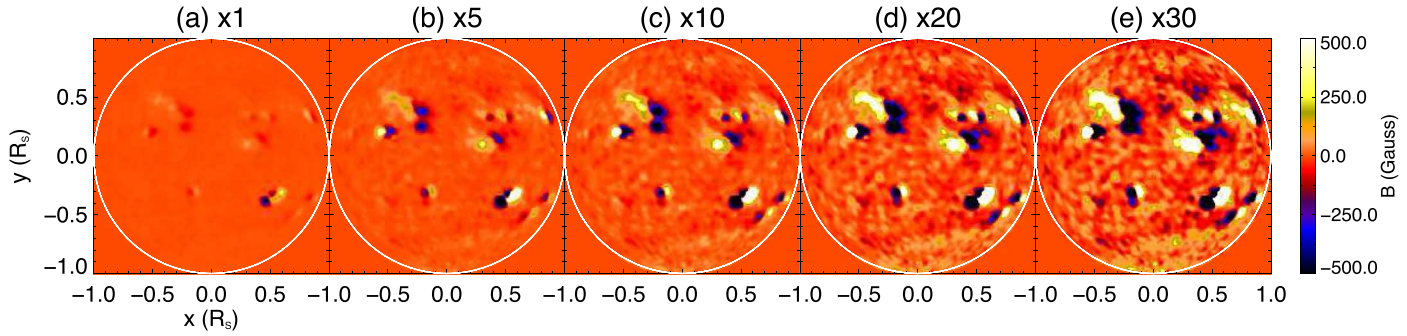

Figure 1. Radial component of the magnetic field at the stellar surface in different models. The $+x$-direction is taken as the LOS. The white circle in each panel indicates the limb of the photosphere.

often several hundred Gauss, which is consistent with the typical field strengths in the lower corona as derived from magnetic field extrapolations (Landi et al. 2020) and magneto-hydrodynamic (MHD) models (Chen et al. 2021).

Here we extend this method to the coronae of other stars through forward modeling with a series of global stellar models. Our investigation suggests that the MIT method could be used to measure the coronal magnetic field for at least a subset of late-type stars.

2. Models and Emission Line Synthesis

We took a series of global MHD models developed by Jin et al. (2020). The global coronae were constructed using the Alfvén Wave Solar Model (AWSoM; van der Holst et al. 2014) within the Space Weather Modeling Framework (SWMF; Tóth et al. 2012). The AWSoM simulation domain starts from the solar upper chromosphere and extends into the corona and heliosphere. A steady-state solar wind solution is obtained with the local time stepping and second-order shock-capturing scheme. The inner boundary condition of the magnetic field is specified by the synchronous magnetogram from an evolving photospheric flux transport model (Schrijver & De Rosa 2003). The inner boundary conditions for electron and proton temperatures T_e and T_i and number density n are assumed to be $T_e = T_i = 50{,}000$ K and $n = 2 \times 10^{17}$ m^{-3}, respectively. The initial conditions for the solar wind plasma are specified by the Parker solution (Parker 1958), while the initial magnetic field is based on the Potential Field Source Surface (PFSS) model. Alfvén waves are driven at the inner boundary with a Poynting flux that scales with the surface magnetic field. The model includes physically consistent treatment of wave reflection, dissipation, and heat partitioning between the electrons and protons. Electron heat conduction (both collisional and collisionless) and radiative cooling are also included in the model.

Specifically, we first constructed a steady-state global model based on the solar synchronous magnetograms (at a resolution of 1°, or ∼17″ at the disk center) obtained from observations of the Helioseismic and Magnetic Imager (HMI; Schou et al. 2012) on board the Solar Dynamics Observatory (SDO) on 2011 February 15, which is in the rising phase of solar cycle 24, and named this solar model the "x1" model. More details of the numerical setups can be found in Jin et al. (2012, 2016) and Oran et al. (2013). Considering that the mean surface magnetic flux densities on many young Sun-like stars and M dwarfs are much higher than that on the Sun (Reiners 2012), we then followed Jin et al. (2020) to construct another four steady-state models by increasing the surface magnetic flux density by factors of 5, 10, 20, and 30, and referred to them as the "x5," "x10," "x20," and "x30" models, respectively.

For each model we took one snapshot of the steady-state global coronal solution for further analyses. We defined the stellar spin axis (i.e., from the stellar center to the polar regions) as the z-direction and chose two orthogonal directions in the equatorial plane as the x- and y-directions. Figure 1 shows the radial component of the magnetic field at the stellar surfaces for a line of sight (LOS) in the $+x$-direction ($+x$ pointing toward the observer). The magnetic field structures on the stellar surface are the same for all models. The maximum magnetic field strength (or more precisely magnetic flux density) on the surface is ∼800 Gauss and the total magnetic flux is $\sim 2 \times 10^{23}$ Mx in the x1 model.

According to the MIT theory, an external magnetic field can increase the transition rate between the Fe X $3p^4\ 3d\ ^4D_{7/2}$ and $3p^5\ ^2P_{3/2}$ levels, leading to enhanced emission of the Fe X 257.261 Å spectral line (Li et al. 2015, 2016). Thus, the intensity ratio of the Fe X 257.261 Å line to an Fe X reference line that is not sensitive to the magnetic field should change with the magnitude of the external magnetic field. In order to perform forward modeling, we first established an atomic database of the Fe X ion. The MIT line Fe X 257.261 Å and the Fe X 257.259 Å line formed through an allowed transition are too close in wavelength, and thus could not be resolved by typical EUV spectrographs with a spectral resolution ranging from several hundred to a few thousand. Because of this, we took the total intensity of these two lines as the intensity of the Fe X 257 Å line. To synthesize the coronal emissions, we followed Chen et al. (2021) and calculated the contribution functions $G(T, n_e, B)$ of the Fe X 174, 175, 177, 184, and 257 Å lines as a function of electron temperature, density, and magnetic field strength (Li et al. 2021).

Stars are usually spatially unresolved when observed from the Earth. So we synthesized the spectral line emissions integrated over the whole star. Since in most observations we can only receive radiation from the Earth-facing side of a star, the integrated emissions will vary with viewing angle. For each model we first selected the $\pm x$-, $\pm y$-, and $\pm z$-directions as six different LOS directions. Emissions from the far side were excluded for each LOS when calculating the intensities I_i (the subscript i refers to the wavelength of one Fe X line in units of angstrom). For each model the intensity of each Fe X line can be calculated as

$$I_i = \int_{V_1} n_e^2 \cdot G_i(T, n_e, B) dV, \quad (1)$$

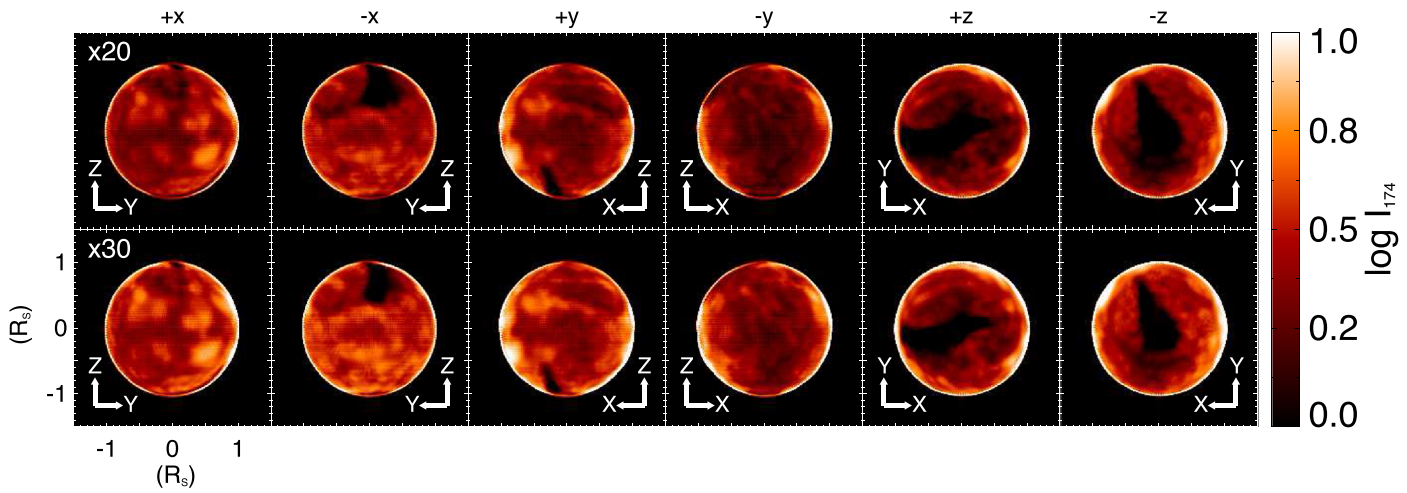

Figure 2. Upper row: synthetic intensity images of the Fe X 174 Å line for the x20 model along different LOS. Lower row: similar to the upper row but for the x30 model. The $\pm z$-directions are parallel to the stellar spin axis. The intensities are shown in logarithm scale and arbitrary units.

where the integration domain V_1 is the whole simulation box excluding the far-side region for each LOS.

For the purpose of understanding the different field strengths obtained from different LOS (see Section 3), we also synthesized the intensity images of the Fe X 174 Å line for the x20 and x30 models along different LOS (Figure 2). The line intensity at every pixel of each image was calculated from Equation (1), where the integration was performed along the corresponding LOS instead of the whole simulation box. Since the magnetic field structures are identical in the photospheres for all the models, their corresponding coronal emission structures are also similar. Comparing the magnetograms shown in Figures 1(d)–(e) to the Fe X emission patterns presented in the first column of Figure 2, we can see a good correspondence, i.e., the coronal emission is enhanced in ARs where the surface magnetic field is stronger. Due to the projection effect and limb brightening of optically thin emission, the ARs near the limb appear to be smaller and brighter in the intensity maps. The intensity maps of other Fe X lines reveal similar patterns.

3. Results and Discussion

Since we used optically thin spectral lines from the Fe X ion to diagnose the magnetic field, a derived field strength should be that weighted by the intensities of these lines. We defined an emissivity-weighted magnetic field strength from the model as:

$$B_{\rm model} = \frac{\int_{V_1} e_{174} \cdot B dV}{\int_{V_1} e_{174} dV}, \quad (2)$$

where $e_{174} = n_e^2 \cdot G_{174}$ is the emissivity of the Fe X 174 Å line, and V_1 corresponds to the whole simulation box excluding the far-side region for a given LOS. To evaluate the accuracy of magnetic field measurements based on the MIT theory, $B_{\rm model}$ will be compared with the field strengths derived from intensity ratios of the synthesized Fe X lines.

According to the MIT theory, the magnetic field strength can be derived from the intensity ratio of Fe X 257 Å to either of the Fe X 174, 177, 184 Å lines (Landi et al. 2020; Si et al. 2020; Chen et al. 2021). Since these line ratios are sensitive to both the magnetic field and electron density (Li et al. 2015), we need

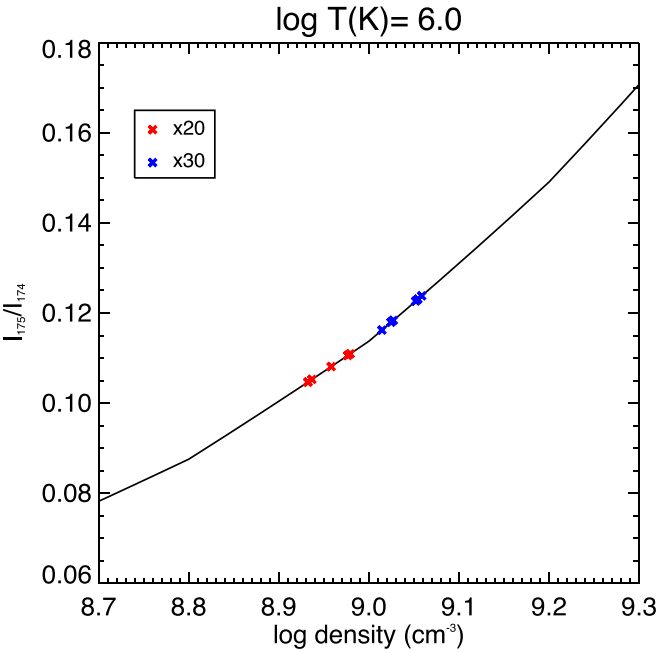

Figure 3. Intensity ratio of the Fe X 175 and 174 Å line pair as a function of electron density. The red and blue crosses indicate the derived densities (along different LOS) for the x20 and x30 models, respectively.

to calculate the density before we can obtain a magnetic field strength from the MIT method. For density diagnostics we took the intensity ratio of the Fe X 174/175 Å line pair, which is sensitive to electron densities of $10^{7.0}$–$10^{10.5}$ cm^{-3} (Brosius et al. 1998; Del Zanna & Mason 2018). The intensity ratio of the Fe X 257/175 Å line pair is much more dependent on the density, and the error of density estimation results in enormous uncertainty of magnetic field measurements. Thus, we did not use the 257/175 Å line pair to derive the magnetic field. For a given LOS in each model, we can obtain a density value from the Fe X 174/175 Å line ratio (I_{175}/I_{174}). As examples, Figure 3 presents the density diagnostic results for the x20 and x30 models. We obtained densities of $10^{8.9–9.0}$ and $10^{9.0–9.1}$ cm^{-3} for the x20 and x30 models, respectively.

For each LOS in a model, with the estimated density and the formation temperature of the Fe X lines (10^6 K), we could

Table 1
Coronal Magnetic Field Strengths Estimated from the Line Ratios I_{257}/I_{174}, I_{257}/I_{177}, and I_{257}/I_{184} for the x20 and x30 Models

	x20				x30			
LOS	$B_{257/174}$	$B_{257/177}$	$B_{257/184}$	$B_{\rm model}$	$B_{257/174}$	$B_{257/177}$	$B_{257/184}$	$B_{\rm model}$
+x	117 (−11%)	115 (−12%)	111 (−15%)	131	176 (−8%)	174 (−9%)	168 (−13%)	192
−x	65 (12%)	64 (10%)	66 (14%)	58	101 (15%)	101 (15%)	92 (5%)	88
+y	116 (−9%)	114 (−11%)	109 (−15%)	128	171 (−8%)	171 (−8%)	162 (−13%)	186
−y	44 (−43%)	42 (−45%)	25 (−68%)	77	171 (47%)	171 (47%)	173 (49%)	116
+z	73 (−21%)	71 (−23%)	63 (−32%)	92	189 (40%)	189 (40%)	190 (41%)	135
−z	59 (−44%)	58 (−45%)	48 (−55%)	106	122 (−21%)	122 (−21%)	113 (−27%)	155

Note. The unit of the magnetic field strength is Gauss. Errors, i.e., differences between the measured field strengths and $B_{\rm model}$, are shown in the brackets.

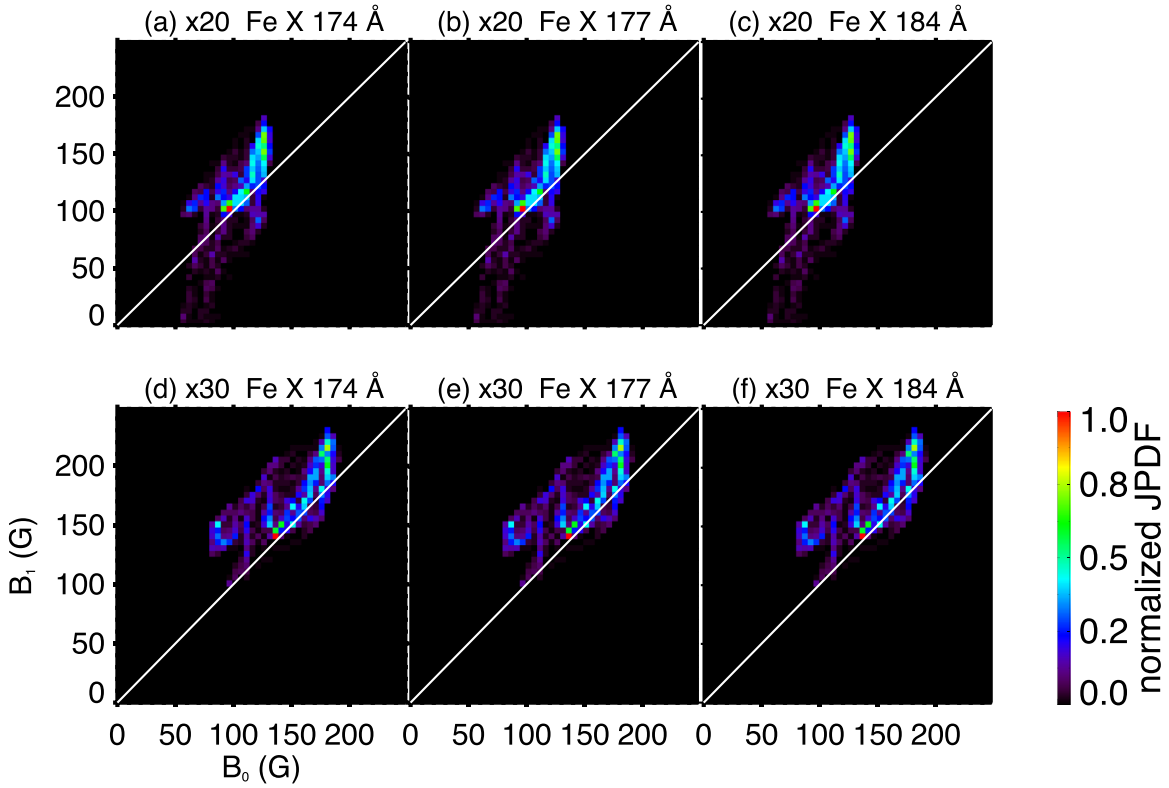

Figure 4. The joint probability density function (JPDF) of coronal magnetic field strengths in the models (B_0) and inferred (B_1) from the intensity ratios of the Fe X 257/174 Å (left panels), 257/177 Å (middle panels), and 257/184 Å (right panels) line pairs based on the MIT method taking different LOS directions. Panels (a)–(c) correspond to the x20 model, and panels (d)–(f) correspond to the x30 model.

calculate the theoretical relationship between I_{257}/I_i (i = 174, 177 or 184) and the magnetic field strength from the Fe X atomic database described in Section 2 (Chen et al. 2021). Using this theoretical relationship, we derived the magnetic field $B_{257/174}$, $B_{257/177}$, and $B_{257/184}$ from the synthesized Fe X line ratios I_{257}/I_{174}, I_{257}/I_{177}, and I_{257}/I_{184}, respectively. The results for the x20 and x30 models are summarized in Table 1. The magnetic field strengths in the models ($B_{\rm model}$) and errors of the magnetic field measurements $(B - B_{\rm model})/B_{\rm model}$ are also included in Table 1.

In the x20 and x30 models, $B_{\rm model}$ changes from several tens to more than 100 Gauss when measured along different LOS. The number of observed ARs changes with LOS as shown in Figure 2, and the magnetic field strengths in ARs are usually much larger than those in the quiet regions. Thus, the magnetic field strengths derived from different LOS in the same model can be different. Then we compared the $B_{\rm model}$ values to the magnetic field strengths derived using the Fe X 257/174, 257/177, and 257/184 Å line pairs. We found that all three Fe X line pairs can provide reasonably accurate estimates of the coronal magnetic field in the models. The differences between the measured field strengths and $B_{\rm model}$ values are mostly smaller than ∼50%, demonstrating that the MIT method can be extended to some late-type stars with strong surface magnetic field fluxes. Furthermore, we selected more LOS directions, i.e., every 5° for both the inclination and azimuth, and derived the magnetic field strengths in the model following Equation (2) (B_0) and inferred from the MIT method (B_1) for each LOS directions. The comparisons between B_0 and B_1 are shown in Figure 4, which do not alter the conclusion mentioned

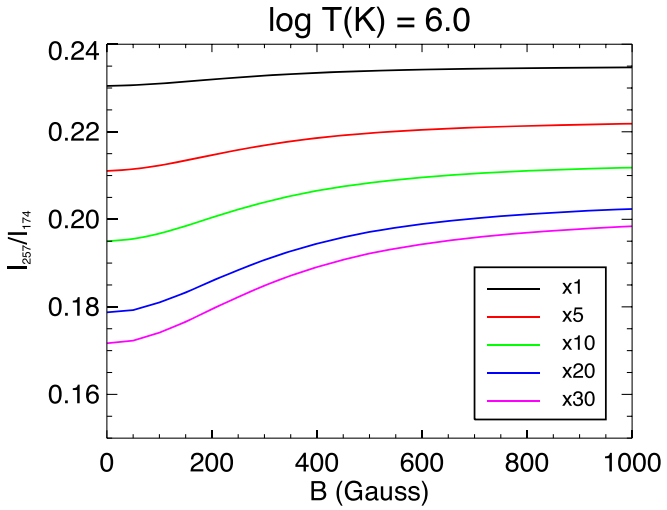

Figure 5. The Fe X 257/174 Å line ratio as a function of the magnetic field strength at the average coronal density (n_0) in each model. The black, red, green, blue, and purple curves represent results for the x1, x5, x10, x20, and x30 models, respectively.

above. So the selection of different LOS directions (thus inclination of the stellar rotation axis with respect to the LOS) does not affect the validation of the MIT method. In addition, we noticed some vertical features in Figure 4. These features do not change much if we use LOS directions with one inclination, suggesting that they are not related to the inclination.

The average coronal temperature in the solar model is $\sim 10^{6.0}$ K. The average coronal temperatures in the x20 and x30 models reach up to $\sim 10^{6.5}$ K (Jin et al. 2020). Considering that the formation temperatures of the Fe X lines peak at $\sim 10^{6.0}$ K, these Fe X lines are likely formed in the upper transition region or coronal base of these models. So the derived field strengths correspond to the magnetic field at the very bottom parts of the stellar coronae. This also explains why the structures of the Fe X line shown in Figure 2 do not extend much above the limb.

However, we found that most values of I_{257}/I_i in the x1, x5, and x10 models do not fall into the ranges predicted by the MIT theory. We have investigated the reasons why this technique fails for the x1, x5, and x10 models. We defined the coronal density in each model as,

$$n_0 = \frac{\int_V e_{174} \cdot n_e dV}{\int_V e_{174} dV}, \quad (3)$$

where the integration volume is the whole calculation domain, without consideration of different LOS. We obtained n_0 values of $10^{8.13}$, $10^{8.58}$, $10^{8.80}$, $10^{8.99}$, and $10^{9.07}$ cm^{-3} for the x1, x5, x10, x20, and x30 models, respectively. Figure 5 shows the Fe X 257 and 174 Å line ratio as a function of the magnetic field strength, taking the density of n_0 in each model. It is obvious that the magnetic field sensitivity of I_{257}/I_{174} becomes worse as the density decreases. For the solar model, I_{257}/I_{174} hardly changes with the magnetic field. Similar results have also been revealed from the Fe X 257/177 and 257/184 Å line ratios. Figure 5 also shows that a density variation can lead to a change in the range of ratios that correspond to the field strengths of 0–1000 Gauss. Because the ranges of ratios are narrower in the low-density x1, x5, and x10 models, a small deviation of the estimated density from the density in the model can cause a given value of synthesized line ratio to fall outside the range of ratios predicted using the estimated density. As a result, a magnetic field strength cannot be inferred for these low-density models.

We noticed that the average coronal density at the Fe X line formation heights of the solar model ($\sim 10^{8.1}$ cm^{-3}) is about one order of magnitude lower than the typical AR density in the lower corona, i.e., $\sim 10^{9.2}$ cm^{-3} as estimated from intensity ratios of density-sensitive Fe XII line pairs in on-disk observations (Tian et al. 2012). It also appears to be a few times lower than the typical quiet-Sun density estimated from on-disk observations of density-sensitive Fe XII and Fe XIII line pairs (Dere et al. 2007). Several reasons could contribute to this issue. (1) Because of the fixed density at the inner boundary of the simulation box, the adopted model lacks the process of chromospheric evaporation resulting from conduction of coronal heating, leading to less plasma in the corona of ARs (Oran et al. 2013). (2) The spatial resolution of the global model is low, so that small-scale dense structures in the lower corona of both the quiet Sun and ARs cannot be well resolved. (3) The temperature in the solar model reaches ~1 MK at larger heights as compared to observations (Oran et al. 2013), meaning that in the model the Fe X lines are formed at larger heights where the density is lower. Consequently, the average density at the Fe X line formation heights of the solar model is lower than that of the real solar corona. Similarly, the average densities in the lower coronae of all the stellar models are likely lower than those of the real stellar coronae. Since the magnetic field sensitivity of the I_{257}/I_i ratio increases with density, we expect that our technique can be extended further to stars with a surface magnetic flux smaller than that in the x20 model. In the near future we plan to quantitatively verify this using stellar models with more realistic coronal densities.

We realized that the scaled magnetograms may not capture the full complexity of the magnetic field on some stars, especially the strong quadrupolar/octopolar components and surface toroidal fields that are present on some young/rapidly rotating stars. However, we think that for the first step of a proof-of-concept investigation, our usage of the scaled magnetograms is still reasonable. This is because the complexity (thus detailed structures) of the stellar magnetic field should not affect the suitability of our technique, as the line ratios of the MIT line and other reference lines are only sensitive to the coronal temperature, density, and magnetic field strength. The average magnetic field strengths (magnetic flux densities) measured on the photospheres of some stars could be up to three orders of magnitude larger than that of the Sun (e.g., Pevtsov et al. 2003; Kochukhov 2021). The larger flux density might be explained by either of the following two scenarios or a combination of the two: (1) a stronger field in regions with typical solar AR sizes, and (2) a larger surface area with a field strength of typical solar AR field strength. In this study, we chose the first scenario since we can make use of the directly observed solar magnetograms. In our x30 model, the maximum field strength is ~25 kG, which should not be too unrealistic if we consider the fact that even the solar photospheric magnetic field can reach ~7.5 kG (van Noort et al. 2013). The second scenario would involve larger sizes of individual ARs or a larger number of ARs. In this situation a photospheric magnetogram at the model inner boundary cannot be easily constructed from actual observations. Nevertheless, in the near

future we plan to construct stellar magnetograms through other approaches, e.g., using stellar flux transport models (Schrijver 2020), and explore the suitability of coronal magnetic field diagnostics with the MIT method.

It is worth mentioning that the interstellar medium could cause absorption of the EUV spectral lines of the Fe X ions we used in this study (Rumph et al. 1994). However, for many stars in the solar neighborhood, the interstellar absorption of these Fe X lines is weak or could be evaluated based on models (France et al. 2019). So as long as these Fe X lines are measured through a future EUV spectrograph, the MIT method can be used to infer the magnetic field strengths at the coronal bases of many nearby stars.

4. Summary

We have proposed a new method to carry out stellar coronal magnetic field measurements using the magnetic-field-induced transition of the Fe X 257 Å line. To investigate the feasibility of this method, we constructed a series of steady-state global stellar models by multiplying the surface magnetic flux density of the real solar observations by factors of 1, 5, 10, 20, and 30 to obtain the x1, x5, x10, x20, and x30 models, respectively. We synthesized the emissions of the Fe X 174, 175, 177, 184, and 257 Å lines, and then derived the coronal electron densities and magnetic field strengths successively using the intensity ratios of different Fe X line pairs for different LOS directions. After that, we compared the derived coronal magnetic field strengths to those in the models.

We found that all the Fe X 257/174, 257/177, and 257/184 Å line ratios can provide reasonably accurate magnetic field measurements at the coronal bases for the x20 and x30 models. Further analyses suggest that the low densities at the lower coronae may have resulted in the failure of the application of this technique for the x1, x5, and x10 models. Our investigation demonstrates that the MIT method can be used to measure the magnetic field strengths at the coronal bases of at least some nearby M dwarfs and young Sun-like stars whose magnetic field strengths are more than one order of magnitude stronger than that of the Sun. To achieve routine measurements of the coronal magnetic field of these stars, an EUV spectrometer that can simultaneously measure at least the Fe X 174, 175, and 257 Å lines is highly desired.

This work is supported by NSFC grants 11825301, 12103066, 11790304, 11704076, 12073004, and U1732140, the Strategic Priority Research Program of CAS (grant No. XDA17040507) and grant 1916321TS00103201.

ORCID iDs

Yajie Chen https://orcid.org/0000-0001-5494-4339
Hui Tian https://orcid.org/0000-0002-1369-1758
Xianyong Bai https://orcid.org/0000-0003-2686-9153
Meng Jin https://orcid.org/0000-0002-9672-3873
Zihao Yang https://orcid.org/0000-0002-4973-0018

References

Alvarado-Gómez, J. D., Drake, J. J., Cohen, O., Moschou, S. P., & Garraffo, C. 2018, ApJ, 862, 93
Argiroffi, C., Reale, F., Drake, J. J., et al. 2019, NatAs, 3, 742
Baranov, V. B. 1990, SSRv, 52, 89
Brooks, D. H., & Yardley, S. L. 2021, SciA, 7, eabf0068
Brosius, J. W., Davila, J. M., & Thomas, R. J. 1998, ApJS, 119, 255
Chen, B., Shen, C., Gary, D. E., et al. 2020, NatAs, 4, 1140
Chen, Y., Tian, H., Su, Y., et al. 2018, ApJ, 856, 21
Chen, Y., Li, W., Tian, H., et al. 2021, ApJ, in press (arXiv:2107.11783)
Del Zanna, G., & Mason, H. E. 2018, LRSP, 15, 5
Dere, K. P., Doschek, G. A., Mariska, J. T., et al. 2007, PASJ, 59, S721
Donati, J.-F., Forveille, T., Collier Cameron, A., et al. 2006, Sci, 311, 633
Dong, C., Lingam, M., Ma, Y., & Cohen, O. 2017, ApJL, 837, L26
Fleishman, G. D., Gary, D. E., Chen, B., et al. 2020, Sci, 367, 278
France, K., Fleming, B. T., Drake, J. J., et al. 2019, Proc. SPIE, 11118, 1111808
Gary, D. E., & Linsky, J. L. 1981, ApJ, 250, 284
Gary, D. E., Chen, B., Dennis, B. R., et al. 2018, ApJ, 863, 83
Güdel, M. 2002, ARA&A, 40, 217
Haisch, B., Strong, K. T., & Rodono, M. 1991, ARA&A, 29, 275
Jardine, M., Collier Cameron, A., & Donati, J. F. 2002, MNRAS, 333, 339
Jin, M., Schrijver, C. J., Cheung, M. C. M., et al. 2016, ApJ, 820, 16
Jin, M., Manchester, W. B., van der Holst, B., et al. 2012, ApJ, 745, 6
Jin, M., Cheung, M. C. M., DeRosa, M. L., et al. 2020, in IAU Proc. 354, Solar and Stellar Magnetic Fields: Origins and Manifestations, ed. A. Kosovichev, S. Strassmeier, & M. Jardine (Cambridge: Cambridge Univ. Press), 426
Johnstone, C. P., Jardine, M., Gregory, S. G., Donati, J. F., & Hussain, G. 2014, MNRAS, 437, 3202
Kochukhov, O. 2021, A&ARv, 29, 1
Kochukhov, O., & Piskunov, N. 2002, A&A, 388, 868
Lammer, H., Lichtenegger, H. I. M., Kolb, C., et al. 2003, Icar, 165, 9
Landi, E., Hutton, R., Brage, T., & Li, W. 2020, ApJ, 904, 87
Landi, E., Li, W., Brage, T., & Hutton, R. 2021, ApJL, 913, L1
Lehmann, L. T., Hussain, G. A. J., Jardine, M. M., Mackay, D. H., & Vidotto, A. A. 2019, MNRAS, 483, 5246
Li, H., Landi Degl'Innocenti, E., & Qu, Z. 2017, ApJ, 838, 69
Li, W., Li, M., Wang, K., et al. 2021, ApJ, 913, 135
Li, W., Grumer, J., Yang, Y., et al. 2015, ApJ, 807, 69
Li, W., Yang, Y., Tu, B., et al. 2016, ApJ, 826, 219
Lin, H., Kuhn, J. R., & Coulter, R. 2004, ApJL, 613, L177
Linsky, J. 2019, Host Stars and their Effects on Exoplanet Atmospheres (Berlin: Springer)
Liu, Y., & Lin, H. 2008, ApJ, 680, 1496
Maehara, H., Shibayama, T., Notsu, S., et al. 2012, Natur, 485, 478
Mutel, R. L., Lestrade, J. F., Preston, R. A., & Phillips, R. B. 1985, ApJ, 289, 262
Oran, R., van der Holst, B., Landi, E., et al. 2013, ApJ, 778, 176
Parker, E. N. 1958, ApJ, 128, 664
Petit, P., Dintrans, B., Solanki, S. K., et al. 2008, MNRAS, 388, 80
Pevtsov, A. A., Fisher, G. H., Acton, L. W., et al. 2003, ApJ, 598, 1387
Reiners, A. 2012, LRSP, 9, 1
Reiners, A., & Basri, G. 2010, ApJ, 710, 924
Rosén, L., Kochukhov, O., & Wade, G. A. 2015, ApJ, 805, 169
Rumph, T., Bowyer, S., & Vennes, S. 1994, AJ, 107, 2108
Schou, J., Scherrer, P. H., Bush, R. I., et al. 2012, SoPh, 275, 229
Schrijver, C. J. 2020, ApJ, 890, 121
Schrijver, C. J., & De Rosa, M. L. 2003, SoPh, 212, 165
Segura, A., Walkowicz, L. M., Meadows, V., Kasting, J., & Hawley, S. 2010, AsBio, 10, 751
Semel, M. 1989, A&A, 225, 456
Si, R., Brage, T., Li, W., et al. 2020, ApJL, 898, L34
Tabataba-Vakili, F., Grenfell, J. L., Grießmeier, J. M., & Rauer, H. 2016, A&A, 585, A96
Tian, H., McIntosh, S. W., Wang, T., et al. 2012, ApJ, 759, 144
Tóth, G., van der Holst, B., Sokolov, I. V., et al. 2012, JCoPh, 231, 870
van der Holst, B., Sokolov, I. V., Meng, X., et al. 2014, ApJ, 782, 81
van Noort, M., Lagg, A., Tiwari, S. K., & Solanki, S. K. 2013, A&A, 557, A24
Veronig, A. M., Odert, P., Leitzinger, M., et al. 2021, NatAs, 5, 697
White, S. M. 1996, in ASP Conf. Ser., 109, Cool Stars, Stellar Systems, and the Sun, ed. R. Pallavicini & A. K. Dupree (San Francisco, CA: ASP), 21
Wiegelmann, T., & Sakurai, T. 2021, LRSP, 18, 1
Yang, Z., Tian, H., Tomczyk, S., et al. 2020a, ScChE, 63, 2357
Yang, Z., Bethge, C., Tian, H., et al. 2020b, Sci, 369, 694
Yokoyama, T., & Shibata, K. 1998, ApJL, 494, L113
Zhao, J., Gibson, S. E., Fineschi, S., et al. 2021, ApJ, 912, 141
Zhao, J., Gibson, S. E., Fineschi, S., et al. 2019, ApJ, 883, 55
Zhu, R., Tan, B., Su, Y., et al. 2021, ScChE, 64, 169